
# Impact of Al profile in high-Al content AlGaN/GaN HEMTs on the 2DEG properties

Applied Physics Letters

RESEARCH ARTICLE | SEPTEMBER 18 2024

# Impact of Al profile in high-Al content AlGaN/GaN HEMTs on the 2DEG properties

A. Papamichail ; A. R. Persson ; S. Richter ; V. Stanishev ; N. Armakavicius ; P. Kühne ; S. Guo ; P. O. Å. Persson ; P. P. Paskov ; N. Rorsman ; V. Darakchieva



*Appl. Phys. Lett.* 125, 123505 (2024)
https://doi.org/10.1063/5.0218911









AIP Publishing

Applied Physics Letters ARTICLE pubs.aip.org/aip/apl

# Impact of Al profile in high-Al content AlGaN/GaN HEMTs on the 2DEG properties

Cite as: Appl. Phys. Lett. **125**, 123505 (2024); doi: 10.1063/5.0218911
Submitted: 14 May 2024 · Accepted: 19 August 2024 ·
Published Online: 18 September 2024



A. Papamichail,[1,a)] A. R. Persson,[1,2] S. Richter,[3] V. Stanishev,[1,4] N. Armakavicius,[1,4] P. Kühne,[1,4] S. Guo,[1] P. O. Å. Persson,[2] P. P. Paskov,[1] N. Rorsman,[5] and V. Darakchieva[1,3,4,a)]

## AFFILIATIONS

[1]Center for III-Nitride Technology, C3NiT—Janzén, Department of Physics, Chemistry and Biology (IFM), Linköping University, SE-58183 Linköping, Sweden
[2]Thin Film Physics, Department of Physics, Chemistry and Biology (IFM), Linköping University, Linköping SE-58183, Sweden
[3]Center for III-Nitride Technology, C3NiT—Janzén, Solid State Physics and NanoLund, Lund University, 221 00 Lund, Sweden
[4]Terahertz Materials Analysis Center, THeMAC, Linköping University, SE-58183 Linköping, Sweden
[5]Department of Microtechnology and Nanoscience, Chalmers University of Technology, SE-41296 Göteborg, Sweden

[a)]**Authors to whom correspondence should be addressed:** alexis.papamichail@liu.se and vanya.darakchieva@ftf.lth.se

## ABSTRACT

Ultra-thin high-Al content barrier layers can enable improved gate control and high-frequency operation of AlGaN/GaN high electron mobility transistors (HEMTs) but the precise composition control is very challenging. In this work, we investigate the compositional profiles of $Al_xGa_{1-x}N$/GaN HEMT structures with targeted Al content in the barrier layer, $x = 0.50$, 0.70, and 1, and thickness in the sub-10 nm range in correlation with the two-dimensional electron gas (2DEG) properties. The HEMT structures are grown by metal-organic chemical vapor deposition on SiC. The maximum Al content in the barrier layer, experimentally determined by scanning transmission electron microscopy combined with energy-dispersive x-ray spectroscopy, is found to be lower than that intended and the deviations from the designed structures increase progressively with increasing $x$. Compositionally sharp interface between GaN and $Al_{0.46}Ga_{0.54}N$ and box-like Al profile is achieved for intended $x \sim 0.50$ while pronounced Al grading is found in the samples with intended $x$ of 0.70 and 1, with a maximum Al content of 0.78 reached for the HEMT structure with intended AlN barrier layer. The impact of the experimentally determined Al profiles on the 2DEG properties, obtained by contactless and electrical Hall effect measurements and coupled with self-consistent solution of the Poisson–Schrödinger equation, is evaluated and discussed. It is shown that the observed deviations from the intended Al profiles have a negative effect on the 2DEG confinement and result in reduced mobility parameters, which have significant implications for the implementation of high-Al content AlGaN/GaN structures in high-frequency devices.





The development of AlGaN/GaN high electron mobility transistor (HEMT) structures for applications in high-frequency and high-power electronics has attracted significant research interest over the last decades.[1–3] The combination of a wider bandgap material (AlGaN) on top of a narrower bandgap material (GaN) leads to the confinement of electrons in the uppermost region of the narrower bandgap material, forming a two-dimensional electron gas (2DEG) with high carrier mobility. Common $Al_xGa_{1-x}N$/GaN HEMT structures typically comprise ~15–25 nm thick barrier layers with $x = 0.25$–0.30, which provide a sheet electron density of $\sim 1 \times 10^{13}$ cm$^{-2}$. Mobilities in the range of ~2200 cm$^2$/Vs or higher have been demonstrated when the channel-to-barrier interface is sharpened during growth or with the addition of a thin AlN interlayer prior the AlGaN barrier growth.[4–7]

High power and ultra-high operational frequencies are enabled by HEMT scaling.[8,9] Particularly, for high-frequency operation the gate length should be scaled down while at the same time, a high gate length/gate-to-channel distance aspect ratio should be maintained in order to avoid parasitic short-channel effects.[10] The latter is achieved by decreasing the gate-to-channel distance, i.e., introducing a thinner barrier layer. The consequent reduction of 2DEG density can be compensated by introducing high-Al content AlGaN (or AlN) ultra-thin barrier layers.[11–14] Increasing the Al content of the AlGaN barrier layer leads to increase in the polarization induced 2DEG density, which in

combination with the high mobility, results in low channel resistance, thus enabling high current density. Furthermore, it allows for achieving similarly high 2DEG densities with reduced layer thickness, which, in turn, enables better gate control and high working frequencies.

Further optimization of high-Al content AlGaN/GaN HEMT devices requires knowledge of the exact Al profile in the barrier layer and its effect on the 2DEG properties. When grown by metal-organic chemical vapor deposition (MOCVD), which is the preferred method for large-scale production, precise control of Al content in the high-Al content barrier becomes very challenging. Recently, Godejohann *et al.*[15] have reported that it was not possible to grow purely binary AlN barrier layer by MOCVD due to enhanced Ga atom diffusion in AlN resulting in the formation of AlGaN with a maximum Al content of 50%–60% and a Gaussian Al profile. The specific Al profile in the barrier layer governs the confinement, charge carrier density, and scattering mechanisms, and hence it is expected to significantly affect the 2DEG properties. However, studies on this topic are very scarce and there is lack of understanding of the impact of the actual Al profiles on the 2DEG properties in high-Al content AlGaN/GaN HEMTs. Determination of the Al content and its profile in such thin barrier layers below 10 nm is rather challenging due to the limited sensitivity of commonly employed techniques such as x-ray diffraction, spectroscopic ellipsometry, and photoluminescence spectroscopy. Consequently, most of the studies related to high-Al content AlGaN/GaN HEMTs consider only nominal/intended Al content in the layers and focus mainly on the device performance.

In this work, we study the effect of Al profile in the barrier layers on the 2DEG properties of $Al_xGa_{1-x}N$/GaN HEMT structures with a nominal $x = 0.5$, 0.7, and 1 grown by MOCVD. The Al profiles are determined by energy-dispersive x-ray spectroscopy (EDS) and scanning transmission electron microscopy (STEM) and are correlated with the 2DEG properties measured by contactless Hall and electrical Hall effect coupled with Poisson–Schrödinger (P–S) simulations. We elaborate on the experimentally determined Al profiles that largely differ from the intended content for $x$ above 0.5, and we discuss possible mechanisms for the observed differences. Potential limitations of MOCVD in relation to the Al content and their implications for implementation of high-Al content AlGaN/GaN HEMTs in high-frequency devices are highlighted.

$Al_xGa_{1-x}N$/GaN HEMT structures with nominal $x = 0.5$, 0.7, and 1 (samples $S_1$, $S_2$, and $S_3$, respectively) were grown by MOCVD by a commercial vendor on semi-insulating 4H-SiC substrates with (0001) orientation. The layer stack included AlN nucleation layer, a GaN buffer layer with an AlGaN backbarrier, GaN channel, AlN interlayer, AlGaN barrier layer, and a GaN cap, as schematically illustrated in Fig. 1. The incorporation of a low-Al content AlGaN backbarrier in a scaled HEMT structure serves for the reduction of short-channel effects and provides better electron confinement in the 2DEG channel by raising the conduction band of the buffer layer with respect to the GaN channel,[16,17] while the thin AlN interlayer that is introduced between the channel and the barrier layer is similarly expected to improve the 2DEG confinement in the GaN channel region.

The Al content profiles and the structural quality were determined by STEM combined with EDS. The measurements were performed using the double corrected Linköping FEI Titan$^3$ 60–300 microscope, operated at 300 kV. The built-in Super-X/QUANTAX EDS system (Bruker) was employed, and the absolute quantifications

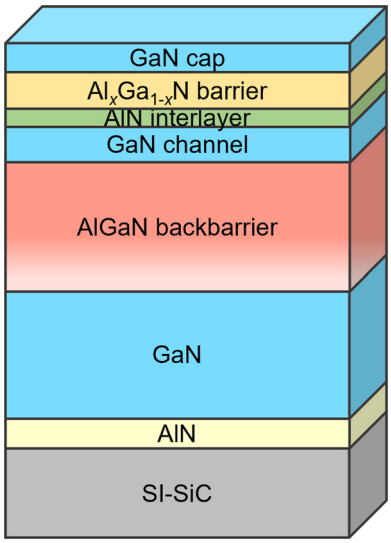


**FIG. 1.** Schematic representation of the layer stack in the $Al_xGa_{1-x}N$/GaN HEMT structures with nominal $x = 0.5$, 0.7, and 1.

were made using the Esprit software and its built-in calibrations for TEM-EDS. Four EDS maps from four different sites were acquired on each sample and integrated along the interface and subsequently quantified. Finally, the profiles were averaged for each sample in order to get more reliable data. This EDS method has recently been demonstrated to deliver reliable estimation of the Al content in ultra-thin AlGaN layers.[7] The 2DEG properties were measured at room temperature using contactless methods. The sheet resistance was obtained by Eddy current-based method using an Eichhorn Hausmann MX604 tool with a working range of 50–3000 Ω/sq. The mobility $\mu$ and sheet electron density $N_s$ were obtained using a microwave (10 GHz) contactless Hall method (Lehighton LEI1600). Van der Pauw structures were fabricated on the same samples for Hall effect measurements. The samples were cleaned with RCA-1, RCA-2, and diluted ammonia to remove organic, metallic contamination, and oxide before deposition of the passivation layer. 15 nm-thick Si-rich silicon nitride ($SiN_x$) passivation layer was deposited at 820 °C by low-pressure chemical vapor deposition.[18] Device isolation is accomplished through mesa-etching. Recessed Ta-based Ohmic contacts are realized with laser writer (Heidelberg Instruments DWL 2000) and evaporation of a Ta/Al/Ta metal stack[19] producing contact resistance of 0.37–0.41 Ω·mm. The measured Al profiles from the quantified EDS measurements were used to simulate band bending and the charge density distribution in the HEMT structures given by the self-consistent solutions of the Poisson and Schrödinger equations. For this purpose, the numerical solver by Snider[20,21] is utilized, employing as input piece-wise linear approximations of the Al profiles according to the measured EDS profiles. The AlN nucleation layer and the SiC substrate were not considered in the simulations. The structural details and the 2DEG properties of all samples are summarized in Table I.

Figure 2 shows the high-resolution STEM images and the corresponding Al profiles obtained from the EDS measurements across the top channel-barrier-cap layers of the samples. The simulated charge density distributions using the measured EDS Al profiles are

**TABLE I.** Structural characteristics and measured 2DEG properties of the studied HEMT structures: the sheet resistance provided by the vendor, the ones measured by Eddy current method and by Hall effect, as well as the 2DEG density and mobility measured by Lehighton and Hall effect. The simulated 2DEG density using the Al profiles measured by EDS is also provided for comparison. The measured barrier layer thickness and peak Al content are determined from the STEM images in Fig. 2.

| Sample | $S_1$ | $S_2$ | $S_3$ |
|---|---|---|---|
| Nominal barrier thickness, $t_b^n$ (nm) | 8.0 | 5.0 | 4.5 |
| Measured barrier thickness, $t_b$ (nm) | 8.2 | 7.1 | 6.1 |
| Nominal Al content | 0.50 | 0.70 | 1.00 |
| Measured peak Al content | 0.46 | 0.64 | 0.78 |
| $R_S$ (Ω/sq) (vendor) | 335 | 431 | 542 |
| $R_S$ (Ω/sq) (Eddy current) | 290 | 370 | 570 |
| $R_S$ (Ω/sq) (Hall) | 298 | 350 | 415 |
| $N_S$ ($\times 10^{13}$ cm$^{-2}$) (Lehighton) | 1.24 | 1.23 | 0.88 |
| $N_S$ ($\times 10^{13}$ cm$^{-2}$) (Hall) | 1.10 | 1.42 | 1.51 |
| $N_S$ ($\times 10^{13}$ cm$^{-2}$) (simulated) | 1.55 | 1.75 | 1.67 |
| $\mu$ (cm$^2$/Vs) (Lehighton) | 1730 | 1390 | 1270 |
| $\mu$ (cm$^2$/Vs) (Hall) | 1775 | 1270 | 1045 |

superimposed on the STEM images. The integrated 2DEG density estimated from the simulated charge density is provided in Table I for comparison. The intended Al content in the barrier layer of sample $S_1$ is 0.5. Apparently, relatively sharp box-like Al profile with adequate control over thickness and composition can be achieved in this case with a slightly lower Al content of 0.46. For samples $S_2$ and $S_3$ with nominal Al content in the barrier of 0.7 and 1.0, respectively, the actual Al profiles become graded. Unlike the box-like profile for the $Al_{0.46}Ga_{0.54}N$ barrier of $S_1$, in $S_2$ and $S_3$ the Al grading starts near the channel–barrier interface and forms a peak deep into the barrier (close to the surface). The peak Al content is determined to be 0.64 for $S_2$ and 0.78 for $S_3$ as neither the intended 70% nor 100% Al compositions, respectively, are reached. At the same time, the barrier area with the peak Al content becomes thinner with increasing Al content (Fig. 2). Such an effect may be expected to some extent as the thickness of the barrier layer is intentionally reduced for the higher Al content structures to not exceed the critical thickness of the nominal Al-containing barrier.

In contrast to earlier reports on AlN/GaN HEMT structures grown by MOCVD, where a Gaussian-shaped Al profile with peak Al content of 0.6 was observed,[15] here we find a clear asymmetric behavior of the Al profiles in the high-Al content AlGaN barrier layers ($S_2$ and $S_3$). In addition, a higher Al content of 0.78 could be achieved for $S_3$. Godejohann *et al.*[15] attributed their Gaussian Al profile to a diffusion of Al atoms from the AlN barrier into the GaN channel and cap layers due to relatively high growth temperatures in the MOCVD process. In our case, Al diffusion is also likely contributing to the observed grading profiles in $S_2$ and $S_3$ (Fig. 2). Since the channel–barrier interface is exposed to the high growth temperatures for a longer period in comparison to the barrier–cap region, the observed lower slope of the Al grading for the former can be expected. This points out the need to keep the growth time of the high-Al content barrier layer as short as possible but without compromising other important properties such as keeping defects and impurities low. Other effects, such as strain-dependent and composition-dependent cation interdiffusion[22,23] and a stress-induced composition pulling,[24] might play a significant role in the formation of graded AlGaN barrier layers. Establishing a direct correlation between growth parameters and Al profiles is very important and will be reported elsewhere for a series of in-house MOCVD-grown high-Al content HEMT structures. We also note that the average Al content determined from x-ray diffraction reciprocal mapping is 0.42, 0.48, and 0.5 for samples $S_1$, $S_2$, and $S_3$, respectively (see the supplementary material, Fig. S1). These averaged values are significantly lower in comparison with the respective peak Al content measured by EDS, which highlights the necessity of complementary characterization techniques to obtain reliable information on Al content in thin graded AlGaN layers.

Another important observation is that in none of the samples the intended ∼1-nm-thick AlN interlayer between barrier and channel could be resolved in the STEM images and the respective EDS Al profiles (Fig. 2). We recall that these nominal AlN interlayers, which are commonly reported in the literature in MOCVD-grown HEMT structures,[25–35] are in fact Al-rich AlGaN layers with Al content of

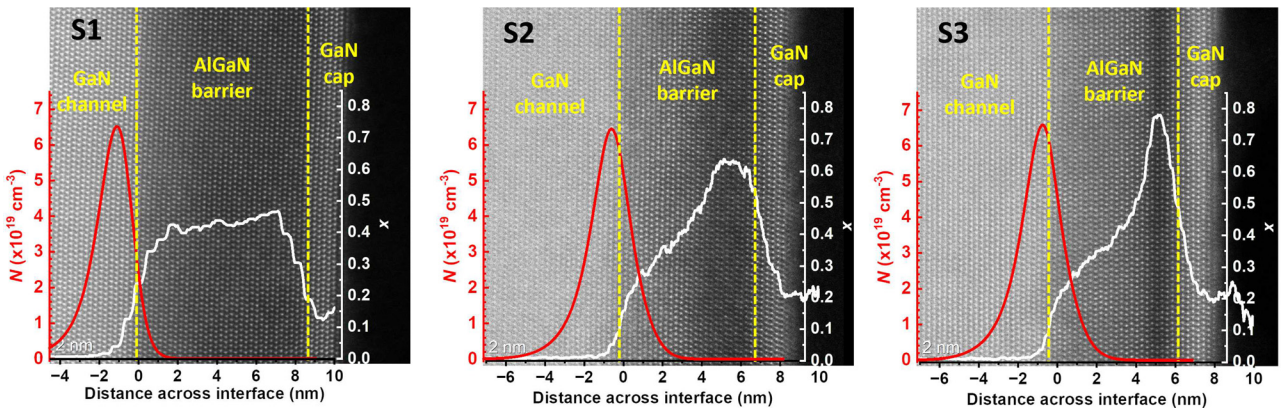


**FIG. 2.** STEM images of the HEMT samples $S_1$-$S_3$ and the corresponding Al content profiles (white) across the top layers in the stack obtained from EDS. The simulated charge density distributions using the measured EDS Al profiles are superimposed on the STEM images (red).

$\sim 0.4 - 0.5$,[4,36–40] as reported previously. Hence, for sample $S_1$ the interlayer would not be distinguishable from the barrier layer with $x \sim 0.50$. However, such an interlayer should be beneficial for achieving a steep compositional transition, which is consistent with the observed relatively sharp onset of the Al content in the barrier layer of this sample. In contrast, as the Al content increases above 0.5 in $S_2$ and $S_3$ with nominal Al content of 0.7 and 1.0, the compositional sharpness is progressively deteriorated with noticeably lower onset of Al content at the interface region between barrier layer and channel. This is expected to reduce the 2DEG confinement and to have a negative impact on the 2DEG properties. The lack of any interlayer in samples $S_2$ and $S_3$ might be potentially explained by a stronger Al diffusion in the higher Al content barriers. More work is needed in order to clarify this.

Furthermore, a low-Al content AlGaN cap layer is observed in all samples instead of the intended GaN cap. For $S_1$ with nominal $x = 0.5$ in the barrier layer, the Al content in the cap is $\sim$ 12% and for $S_2$ and $S_3$ it is $\sim$ 20%. Similar observations have been reported earlier for MOCVD AlN/GaN HEMT structures.[15] The Al atoms in the nominally pure GaN cap layer may originate from delayed incorporation from the gas phase or Al diffusion from the AlGaN barrier layer beneath.[23,41]

The Al profile in the barrier layer as well as the maximum content reachable will significantly affect the 2DEG distribution and hence the HEMT properties. Samples $S_1$ and $S_2$ have similar sheet electron density $\sim 1.2 \times 10^{13}$ cm$^{-2}$ (Table I), which results though from different Al-profile line shapes, with a thicker and lower Al content barrier in the case of sample $S_1$ ($t_b = 8.2$ nm, x $\sim$ 0.46) and a thinner but higher Al content barrier in the case of sample $S_2$ ($t_b = 7.1$ nm, x $\sim$ 0.64). In the case of sample $S_3$ with intended AlN barrier, the measured $N_S = 8.8 \times 10^{12}$ cm$^{-2}$ obtained using the contactless Hall (Lehighton) method is $\sim$ 53% of that expected from the simulation (see Table I). This discrepancy can be attributed to the sample size, which is smaller than the optimal size for the measurement method. Indeed, the results from Hall effect measurements show $N_S = 1.51 \times 10^{13}$ cm$^{-2}$ for $S_3$, which is much closer to the value of $1.67 \times 10^{13}$ cm$^{-2}$ estimated from the simulations (Table I). An overall fair agreement between the respective 2DEG densities obtained from the contactless Hall method, the electrical Hall method, and those estimated based on the simulations is observed for $S_1$ and $S_2$.

A stronger effect of the Al profile line shape is seen on the 2DEG mobility (Table I). As the peak Al content increases and the grading in the barrier layer becomes more pronounced (Fig. 2), a greater portion of the electron density wavefunction penetrates into the AlGaN barrier layer. Consequently, a larger fraction of the electrons faces extensive alloy disorder scattering,[42] which results in decreased mobilities from 1730 cm$^2$/Vs in $S_1$ to 1390 cm$^2$/Vs in $S_2$ and to 1270 cm$^2$/Vs in $S_3$ (Table I, contactless Hall–Lehighton method[43]). Apparently, the absence of AlN interlayer and sharp compositional channel-to-barrier transition leads to weaker confinement of the 2DEG in the GaN channel and, hence, reduces the mobility. The fraction of electron volume density penetrating the AlGaN barrier increases from $\sim$7% for $S_1$ to $\sim$37% for $S_3$ as calculated from Fig. 2 (percentage of the integrated area under the simulated charge density plot penetrating the barrier layer). In addition to the reduction due to alloy disorder scattering, mobility can also be reduced due to increase in the effective mass parameter. We have estimated the enhancement of effective mass, $m^*$, due to the penetration of electron density wavefunction into the AlGaN barrier layer following Refs. 44 and 45 and using $m^* = 0.232\, m_0$[46] for GaN and $m^* = 0.364\, m_0$[47] for AlN. The resulting hybridized effective mass $m^*_{hyb}$ increases from $0.234\, m_0$ to $0.243 m_0$ as shown in Fig. 3. Such an enhancement of the effective mass, although moderate, has a negative impact as it inherently limits the maximum mobility. We note, however, that there are stronger enhancement mechanisms such as the polaron effect in GaN, which is constant for all samples, and the conduction band non-parabolicity effect,[48] which is sample dependent (as $n_s$ depends on the thickness and composition of the barrier layer). The enhancement of the 2DEG effective mass due to these different mechanisms as well as their combined effect is shown for the HEMT structures $S_1$–$S_3$ in Fig. 3. The 2DEG effective mass increase due to all effects combined $m^*_{comb}$ is comparable (0.28–0.29) for all three samples (Fig. 3) and hence cannot account for the observed significant decrease in mobility with increasing Al content in the barrier layer. We also note that the $Al_xGa_{1-x}N$ surface root mean square (RMS) roughness is not affected by the increasing Al content in the barrier layer and it is within the range of $0.2 - 0.3$ nm over $10 \times 10\ \mu m^2$ area (see the supplementary material, Fig. S2). This implies that the interface roughness between the high-Al content barrier and GaN is not degrading as also inferred from TEM (see the supplementary material, Fig. S3). The high crystalline quality of epilayers for all structures is further confirmed by XRD and RSM (see the supplementary material, Figs. S1 and S4). Hence, degradation of structural quality with increasing Al content in the barrier could also be excluded as a reason for the observed decrease in 2DEG mobility parameters. Instead, we suggest that this can be rather explained by an increase in alloy scattering with increasing $x$. This is consistent with the STEM and EDS results (Fig. 2) revealing progressively stronger grading with increase in the intended $x$, i.e., from no grading in $S_1$, to grading from 0.20 to 0.64 for $S_2$ and from 0.20 to 0.78 for $S_3$. These observations are particularly important for the transport properties of HEMT structures intended for high-frequency applications.

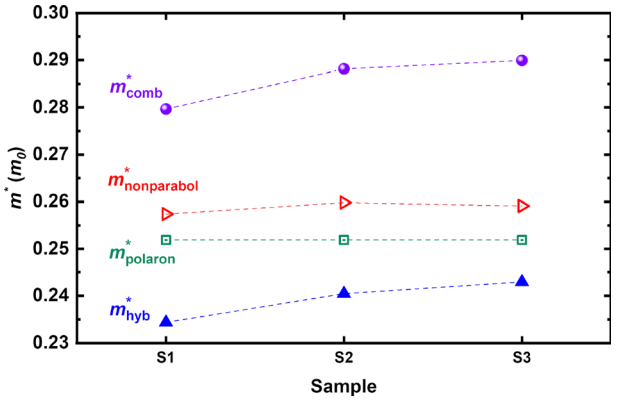


**FIG. 3.** Estimated 2DEG effective mass $m^*$ parameter for the HEMT samples $S_1$–$S_3$ taking into account (i) the hybridization due to 2DEG penetration in the barrier layer (filled triangles), (ii) the conduction band non-parabolicity effect (empty triangles), (iii) the polaron effect (squares)—constant as a function of Al content, and (iv) the combination of all effects (spheres).

In order to gain further understanding of how the 2DEG properties are affected by the actual Al content profiles and structure layout in the samples, we compare in Fig. 4 the simulated conduction band profiles and the electron density distributions for the designed nominal

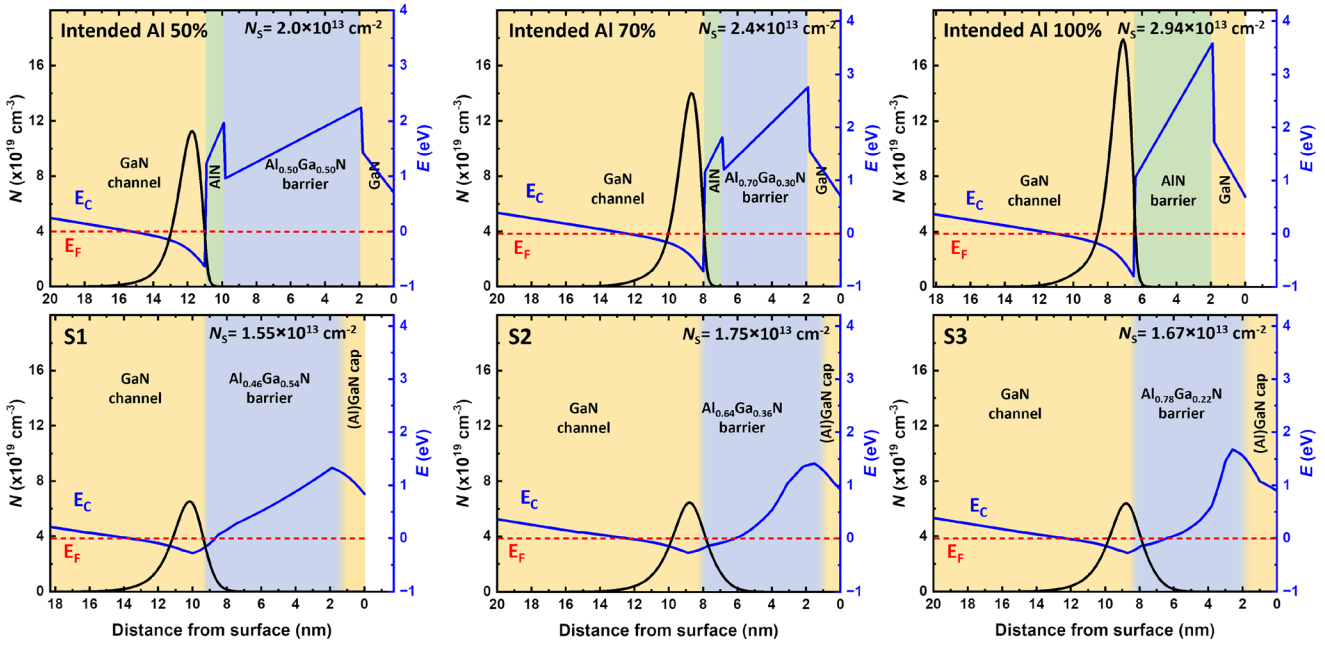


**FIG. 4.** Simulations of the conduction band profile and the electron density distribution in the intended structures with nominal Al contents and thicknesses (top row), compared to the corresponding simulations for $S_1$, $S_2$, and $S_3$ according to the Al profiles measured by EDS (bottom row). The integrated 2DEG sheet density, $N_s$, is also shown in both cases.

layer thicknesses and Al content (upper row) with the respective experimentally measured counterparts (bottom row). The nominal structures have identical layout up to the AlN interlayer (see Fig. 1) and they differ in terms of Al content and thickness of the barrier layer (see Table I). As expected, the presence of AlN interlayer (intended structures) creates an abrupt bending of the conduction band and formation of a deep well in GaN, while the strong polarization field between AlN and GaN is responsible for the high electron density (on the order of $10^{20}$ cm$^{-3}$) near the interface. The integrated sheet electron density of samples $S_1$, $S_2$, and $S_3$ estimated using the EDS-measured Al profiles is ∼23%, ∼27%, and ∼43% lower than the corresponding value for the structures with nominal box profiles with Al content $x = 0.50$, 0.70, and 1.00, respectively. Comparing the measured $N_s$ (Table I) with the corresponding simulated values for the intended structures (box-like Al profiles and nominal Al content) results in even larger deviations, with lower $N_s$ of ∼38%, ∼49%, and ∼70%, respectively. This is in part responsible for the increase in sheet resistance as the Al content in the barrier is increased from $S_1$ to $S_3$ (see in Table I). The deviations from the nominal Al content profile also negatively impact the 2DEG confinement (Fig. 4) and lead to decrease in mobility as discussed above. These deviations of the physical parameters of the AlGaN barrier (thickness and Al content) from the designed parameter values are expected to affect the gate control and electron transport properties of the HEMT and consequently its maximum oscillation frequency $f_{max}$. Due to the inherently high temperatures employed in MOCVD, diffusion of Al could be difficult to control. Further investigations are required to fully understand the growth mechanisms limiting the Al incorporation and the lack of abrupt interfaces in MOCVD-grown high-Al content AlGaN on GaN.

In summary, we have determined the Al profiles in high-Al content $Al_xGa_{1-x}N$/GaN HEMT structures with intended $x = 0.5$, 0.7, and 1 grown by MOCVD in relation to their 2DEG properties. It is shown that the Al profile, experimentally determined by EDS, is substantially altered from the intended design when the Al content in the barrier exceeds $x = 0.5$. While $Al_{0.5}Ga_{0.5}N$/GaN HEMT structures with compositionally and structurally sharp interfaces can be readily demonstrated, further increase in Al content beyond 0.5 results in pronounced compositional grading. A maximum Al content of 0.78 is reached for the HEMT structure with intended AlN barrier layer. However, the progressively deteriorating compositional sharpness leads to reduced 2DEG confinement and decreased mobility as a result of alloy disorder scattering. The results of this study stress the need for in-depth structural properties characterization to be undertaken during the optimization of the MOCVD growth of high-frequency oriented HEMT structures.

See the supplementary material for additional details about (*i*) the XRD reciprocal space maps, (ii) the surface morphology (AFM images), (iii) additional STEM images of the structures, and (iv) dislocation densities as estimated from XRD, for the studied samples, as well as the measured and simulated $N_s$ values according to the EDS-measured and the intended-nominal Al profiles.

This work is performed within the framework of the competence center for III-Nitride technology, C3NiT—Janzén supported by the Swedish Governmental Agency for Innovation Systems (VINNOVA) under the Competence Center Program Grant No. 2022-03139, Lund University, Linköping University,

Chalmers University of Technology, Ericsson, Veeco SiC CVD systems, FMV, Gotmic, Hexagem, Hitachi Energy, ON Semiconductor, Region Skåne SAAB, SweGaN, Volvo Cars, and UMS. We further acknowledge support from the Swedish Research Council VR under Award Nos. 2016-00889 and 2022-04812, Swedish Foundation for Strategic Research under Grant Nos. RIF14-055, EM16-0024, and STP19-0008 and the Swedish Government Strategic Research Area in Materials Science on Functional Materials at Linköping University, Faculty Grant SFO Mat LiU No. 2009-00971. The KAW Foundation is also acknowledged for the support of the Linköping Electron Microscopy Laboratory. P. O. Å. Persson acknowledges ARTEMI, the Swedish National Infrastructure in Advanced Electron Microscopy, through funding from the Swedish Research Council and the Foundation for Strategic Research (Grant Nos. 2021-00171 and RIF21-0026).

## AUTHOR DECLARATIONS

### Conflict of Interest

The authors have no conflicts to disclose.

### Author Contributions

**A. Papamichail:** Conceptualization (equal); Data curation (lead); Formal analysis (lead); Investigation (lead); Visualization (equal); Writing – original draft (equal); Writing – review & editing (equal). **A. R. Persson:** Formal analysis (equal); Investigation (equal); Writing – review & editing (equal). **S. Richter:** Formal analysis (equal); Investigation (equal); Writing – review & editing (equal). **V. Stanishev:** Formal analysis (equal); Investigation (equal). **N. Armakavicius:** Formal analysis (equal); Investigation (equal). **P. Kühne:** Formal analysis (equal); Investigation (equal). **S. Guo:** Formal analysis (supporting); Investigation (supporting). **P. O. Å. Persson:** Supervision (equal); Writing – review & editing (equal). **P. P. Paskov:** Investigation (equal); Validation (equal); Writing – review & editing (equal). **N. Rorsman:** Conceptualization (equal); Formal analysis (equal); Investigation (equal); Methodology (equal); Resources (equal); Supervision (equal); Validation (equal); Writing – review & editing (equal). **V. Darakchieva:** Conceptualization (equal); Funding acquisition (lead); Investigation (supporting); Methodology (equal); Project administration (lead); Resources (equal); Supervision (lead); Validation (equal); Writing – review & editing (lead).

## DATA AVAILABILITY

The data that support the findings of this study are available from the corresponding authors upon reasonable request.

## REFERENCES

[1]Y. Tang, K. Shinohara, D. Regan, A. Corrion, D. Brown, J. Wong, A. Schmitz, H. Fung, S. Kim, and M. Micovic, IEEE Electron Device Lett. **36**, 549–551 (2015).
[2]A. Margomenos, A. Kurdoghlian, M. Micovic, K. Shinohara, D. Brown, A. Corrion, H. Moyer, S. Burnham, D. Regan, R. Grabar *et al.*, in *IEEE Compound Semiconductor Integrated Circuit Symposium (CSICS)* (IEEE, 2014).
[3]K. Harrouche, R. Kabouche, E. Okada, and F. Medjdoub, in *IEEE/MTT-S International Microwave Symposium (IMS)* (IEEE, 2020), pp. 285–288.
[4]J.-T. Chen, I. Persson, D. Nilsson, C.-W. Hsu, J. Palisaitis, U. Forsberg, P. O. Å. Persson, and E. Janzén, Appl. Phys. Lett. **106**, 251601 (2015).
[5]N. Armakavicius, J.-T. Chen, T. Hofmann, S. Knight, P. Kühne, D. Nilsson, U. Forsberg, E. Janzén, and V. Darakchieva, Phys. Status Solidi C **13**, 369 (2016).
[6]J. Chu, Q. Wang, L. Jiang, C. Feng, W. Li, H. Liu, H. Xiao, and X. Wang, J. Electron. Mater. **50**, 2630–2636 (2021).
[7]A. Papamichail, A. R. Persson, S. Richter, P. Kühne, V. Stanishev, P. O. Å. Persson, R. Ferrand, Drake D. Castillo, M. Thorsell, H. Hjelmgren, P. Paskov *et al.*, Appl. Phys. Lett. **122**, 153501 (2023).
[8]K. Shinohara, D. C. Regan, Y. Tang, A. L. Corrion, D. F. Brown, J. C. Wong, J. F. Robinson, H. H. Fung, A. Schmitz, T. C. Oh, S. J. Kim, P. S. Chen, R. G. Nagele, A. D. Margomenos, and M. Micovic, IEEE Trans. Electron Devices **60**, 2982–2996 (2013).
[9]K. Shinohara, in *III-Nitride Electronic Devices*, Semiconductors and Semimetals Vol. 102, edited by R. Chu and K. Shinohara (Elsevier, 2019), pp. 141–184.
[10]E. Dogmus, R. Kabouche, A. Linge, E. Okada, M. Zegaoui, and F. Medjdoub, Phys. Status Solidi A **214**, 1600797 (2017).
[11]A. Hickman, R. Chaudhuri, L. Li, K. Nomoto, N. Moser, M. Elliott, M. Guidry, K. Shinohara, J. C. M. Hwang, H. G. Xing, and D. Jena, Phys. Status Solidi A **220**, 2200774 (2023).
[12]J. G. Felbinger, M. Fagerlind, O. Axelsson, N. Rorsman, X. Gao, S. Guo, W. J. Schaff, and L. F. Eastman, IEEE Electron Device Lett. **32**, 889–891 (2011).
[13]I. Smorchkova, S. Keller, S. Heikman, C. Elsass, B. Heying, P. Fini, J. Speck, and U. Mishra, Appl. Phys. Lett. **77**, 3998–4000 (2000).
[14]Y. Cao and D. Jena, Appl. Phys. Lett. **90**, 182112 (2007).
[15]B.-J. Godejohann, E. Ture, S. Müller, M. Prescher, L. Kirste, R. Aidam, V. Polyakov, P. Brückner, S. Breuer, K. Köhler, R. Quay, and O. Ambacher, Phys. Status Solidi B **254**, 1600715 (2017).
[16]R. Kabouche, J. Derluyn, R. Pusche, S. Degroote, M. Germain, R. Pecheux, E. Okada, M. Zegaoui, and F. Medjdoub,in *13th European Microwave Integrated Circuits Conference (EuMIC)* (IEEE, 2018), pp. 5–8.
[17]F. Medjdoub, M. Zegaoui, B. Grimbert, N. Rolland, and P.-A. Rolland, Appl. Phys. Express **4**, 124101 (2011).
[18]D.-Y. Chen, A. R. Persson, K.-H. Wen, D. Sommer, J. Grünenpütt, H. Blanck, M. Thorsell, O. Kordina, V. Darakchieva, P. O. Å. Persson, J.-T. Chen, and N. Rorsman, Semicond. Sci. Technol. **37**, 035011 (2022).
[19]R. Ferrand-Drake Del Castillo, D.-Y. Chen, J.-T. Chen, M. Thorsell, V. Darakchieva, and N. Rorsman, IEEE Trans. Electron Devices **71**, 3596 (2024).
[20]I. Tan, G. L. Snider, L. D. Chang, and E. L. Hu, J. Appl. Phys. **68**, 4071 (1990).
[21]G. L. Snider, see https://www3.nd.edu/~gsnider/ for a program for solving one-dimensional Poisson and Schrodinger equations self-consistently.
[22]M. Nemoz, F. Semond, S. Rennesson, M. Leroux, S. Bouchoule, G. Patriarche, and J. Zuniga-Perez, Superlattices Microstruct. **150**, 106801 (2021).
[23]N. Chaaben, J. Laifi, H. Bouazizi, C. Saidi, A. Bchetnia, and B. El Jani, Mater. Sci. Semicond. Process. **42**, 359–363 (2016).
[24]B. Liu, R. Zhang, J. Zheng, X. Ji, D. Fu, Z. Xie, D. Chen, P. Chen, R. Jiang, and Y. Zheng, Appl. Phys. Lett. **98**, 261101 (2011).
[25]X. Wang, S. Huang, Y. Zheng, K. Wei, X. Chen, H. Zhang, and X. Liu, IEEE Trans. Electron Devices **61**, 1341–1346 (2014).
[26]H. Wang, H. Chiu, W. Hsu, C. Liu, C. Chuang, J. Liu, and Y. Huang, Coatings **10**, 570 (2020).
[27]J. Chen, J. Qin, X. Ma, and H. Wang, Solid-State Electron. **202**, 108619 (2023).
[28]D. Marti, S. Tirelli, A. R. Alt, J. Roberts, and C. R. Bolognesi, IEEE Electron Device Lett. **33**, 1372–1374 (2012).
[29]Y. Zhang, Y. Dong, K. Chen, K. Dang, Y. Yao, B. Wang, J. Ma, W. Liu, X. Wang, J. Zhang *et al.*, Appl. Phys. Lett. **122**, 191701 (2023).
[30]R. Wang, P. Saunier, X. Xing, C. Lian, X. Gao, S. Guo, G. Snider, P. Fay, D. Jena, and H. Xing, IEEE Electron Device Lett. **31**, 1383–1385 (2010).
[31]D. S. Lee, X. Gao, S. Guo, D. Kopp, P. Fay, and T. Palacios, IEEE Electron Device Lett. **32**, 1525–1527 (2011).
[32]P. Cui and Y. Zeng, Sci. Rep. **12**, 16683 (2022).
[33]S. Ozaki, J. Yaita, A. Yamada, Y. Kumazaki, Y. Minoura, T. Ohki, N. Okamoto, N. Nakamura, and J. Kotani, Appl. Phys. Express **14**, 041004 (2021).
[34]A. Yamada, J. Yaita, N. Nakamura, and J. Kotani, J. Cryst. Growth **560**, 126046 (2021).
[35]C. Manz, S. Leone, L. Kirste, J. Ligl, K. Frei, T. Fuchs, M. Prescher, P. Waltereit, M. A. Verheijen, A. Graff *et al.*, Semicond. Sci. Technol. **36**, 034003 (2021).

[36]S. Dai, H. Gao, Y. Zhou, Y. Zhong, J. Wang, J. He, R. Zhou, M. Feng, Q. Sun, and H. Yang, J. Phys. D **51**, 035102 (2017).
[37]Q. Li and Y. Zhang, AIP Adv. **13**, 015214 (2023).
[38]A. Malmros, J.-T. Chen, H. Hjelmgren, J. Lu, L. Hultman, O. Kordina, E. Ö. Sveinbjörnsson, H. Zirath, and N. Rorsman, IEEE Trans. Electron Devices **66**, 2910–2915 (2019).
[39]B. Mazumder, S. W. Kaun, J. Lu, S. Keller, U. K. Mishra, and J. S. Speck, Appl. Phys. Lett. **102**, 111603 (2013).
[40]J. Lu, Y.-L. Hu, D. F. Brown, F. Wu, S. Keller, J. S. Speck, S. P. DenBaars, and U. K. Mishra, Jpn. J. Appl. Phys., Part 1 **51**, 115502 (2012).
[41]D. Cai, X. Chen, H. Xu, N. Lin, F. Xu, and H. Chen, Jpn. J. Appl. Phys., Part 1 **52**, 08JB30 (2013).
[42]M. E. Coltrin, A. G. Baca, and R. J. Kaplar, ECS J. Solid State Sci. Technol. **6**, S3114 (2017).
[43]Similar trend is observed also for the mobilities measured by Hall effect.
[44]A. Kurakin, S. Vitusevich, S. Danylyuk, H. Hardtdegen, N. Klein, Z. Bougrioua, A. Naumov, and A. Belyaev, J. Appl. Phys. **105**, 073703 (2009).
[45]S. Knight, S. Richter, A. Papamichail, P. Kühne, N. Armakavicius, S. Guo, A. R. Persson, V. Stanishev, V. Rindert, P. O. Å. Persson, P. P. Paskov, M. Schubert, and V. Darakchieva, J. Appl. Phys. **134**, 185701 (2023).
[46]A. Kasic, M. Schubert, S. Einfeldt, D. Hommel, and T. E. Tiwald, Phys. Rev. B **62**, 7365 (2000).
[47]S. Schöche, T. Hofmann, D. Nilsson, A. Kakanakova-Georgieva, E. Janzén, P. Kühne, K. Lorenz, M. Schubert, and V. Darakchieva, J. Appl. Phys. **121**, 205701 (2017).
[48]P. Kühne, N. Armakavicius, A. Papamichail, D. Q. Tran, V. Stanishev, M. Schubert, P. P. Paskov, and V. Darakchieva, Appl. Phys. Lett. **120**, 253102 (2022).